Journal of Nuclear Materials 382 (2008) 176–183

Contents lists available at ScienceDirect

Journal of Nuclear Materials

journal homepage: www.elsevier.com/locate/jnucmat

Changes in the mechanical properties of irradiated MgO(100) crystals investigated by nanoindentation and computer simulation

Asta Richter [a,*], Ismail Gheewala [b], Roger Smith [b], Steven D. Kenny [b], James Valdez [c], Kurt Sickafus [c]

[a] Department of Engineering, University of Applied Sciences Wildau, Bahnhofstrasse 1, 15745 Wildau, Germany
[b] Department of Mathematical Sciences, Loughborough University, Loughborough LE11 3TU, UK
[c] MST8, Los Alamos National Laboratory, Los Alamos, NM 87545, USA

ARTICLE INFO

PACS:
62.20.−x
61.80.Az
61.43.Bn

ABSTRACT

This paper presents a nanoindentation study of MgO(100) crystals by experiment and molecular dynamics simulations. The MgO crystals are Ar^+ irradiated up to a fluence of 10^{20} Ar^+/m^2. The materials are compared both before and after irradiation by nanoindentation confirming an increase in hardness but not in the indentation modulus with increasing dose. The experimental and simulation results also indicate that radiation induced defect pinning decreases the dislocation mobility to increase hardness and to cause the material to become less brittle. Molecular dynamic simulation studies confirm the experimental observation for non-irradiated magnesia of pop-in events and slip occurring in the (110) planes which can result in pile up patterns after indentation which are dependent on crystal orientation. The slip systems can cause the injection of half planes into the upper layers, that often retract after tip removal. This feature can be attributed to the formation and partial recombination of nanocracks.

1. Introduction

Magnesia is a widely used material for many applications such as thin film fabrication (substrates for film deposition of high T_c superconductors and compound semiconductors) and applied optics. As a simple ionic representative of the rock salt structure the mechanical properties of MgO have been widely studied. Its intrinsic brittleness, however, complicates macroscopic deformation at room temperature, so that uniaxial tension or compression experiments are not especially easy to perform. On the other hand, small and medium load indentation offers easy access to the mechanical properties of MgO [1–7]. Typical features of mechanical deformation of MgO crystals during micro and nanoindentation include purely elastic deformation, pop-ins, elasto-plastic processes and crack formation. Indentation cracking behaviour and hardness of different MgO crystal orientations (100), (110) and (111) have been studied with fairly high loads up to 130 N [1,2]. A strong dependence on the crystal orientation was observed. Nanoindentation using a scanning force microscopy (SFM) instrument on a very small scale was carried out using a silicon tip with a radius of 10 nm and with an applied force of up to 2.5 μN [5]. Plastic deformation is indicated by discrete events in the indentation curve, which are associated with the number of atomic layers being expelled by the tip penetrating the surface. After every discontinuity in the load–depth curve elastic deformation occurs again with the same slope as in the beginning indicating that further compression up to a critical pressure is necessary to expel more sets of atomic planes. Dislocations were not seen to be generated.

Nanoindentation experiments with loads up to 700 mN have been performed on pure and doped MgO crystals and neutron irradiated MgO crystals [3,4,6,7]. A hardness increase was reported for irradiated samples. Caceres et al. [6] attributed the hardness rise to oxygen interstitials. Tromas et al. [3] describe non-irradiated plasticity in MgO with the nucleation of interstitial dislocation loops followed by the development of a complex dislocation system, whereas in [7] a model of point defect assisted plasticity was proposed.

Atomistic modelling of mechanical behaviour [8] and molecular dynamic simulations of the nanoindentation process [9,10] have been reported in the literature for metals and semiconductors, but the mechanisms of plastic deformation of MgO crystals during nanoindentation has not been studied so far by molecular dynamics (MD) simulations. Since MgO is modelled as an ionic material with fixed charges, the long range Coulomb sums mean that the calculations are more computationally intensive than for the other materials. The investigations in this paper focus to a comparison between the computer simulations on MgO(100) and experiments to explain the mechanism of mechanical deformation in a clear way. Since cracking is a typical feature of a brittle material, the investigation of the possible development of nano-cracks is one of the objectives of the work.

* Corresponding author. Tel.: +49 3375 508219; fax: +49 3375 508238.
E-mail address: asta.richter@tfh-wildau.de (A. Richter).

0022-3115/$ - see front matter © 2008 Elsevier B.V. All rights reserved.
doi:10.1016/j.jnucmat.2008.08.023

2. Experimental

2.1. Materials

The MgO single crystals were purchased from Coating and Crystal Technology, Kittanning, PA, USA. The company provided a material specification with the following features: the MgO single crystals are 99.9% pure, free of air bubbles and free of twinning and strain defects. The MgO crystals do not contain doping elements and are not covered with a special coating. They have not been heat treated and were kept in a sealed box to avoid moisture damage.

The crystals with different orientations are polished to a surface roughness smaller than 0.2 nm measured by scanning force microscopy at a scan size of 125 μm × 125 μm. The mechanical properties of these pristine MgO single crystals and MgO crystals after ion irradiation are studied by nanoindentation.

MgO single crystals were irradiated at room temperature with 100 keV Ar^+ ions to fluences of 5×10^{19} Ar^+/m^2 and 1×10^{20} Ar^+/m^2. To avoid channelling the irradiation was performed at an angle of 7° off normal. The Ar^+-irradiation was performed using a 200 kV Varian implanter. Ballistic damage and the implanted Ar atomic concentration as a function of depth into the target was obtained from the Monte Carlo code SRIM2000 [11] for the highest ion fluence 1×10^{20} Ar^+/m^2 used in these experiments. These data were obtained using displacement energies of 40 eV for both Mg and O atoms and a density of 3.58×10^{-3} kg/m^3. Peak damage of 9 dpa (displacements per atom) at 52 nm and a peak Ar^+ ion concentration of approximately 2% at about 72 nm were predicted using the code SRIM2000 with ions penetrating up to a maximum depth of 150 nm. No amorphisation or bubble formation could be detected after irradiation.

2.2. Nanoindentation

Depth sensing nanoindentation [12–15] differs from classical hardness measurements (Vickers, Brinell and Knoop), where the impressions are first generated, and then imaged using a microscopy technique. Load and penetration depth are simultaneously recorded during both loading and unloading, resulting in a load–displacement diagram. This diagram provides much more information than a microscopy image of the impression since it provides the elastic and plastic deformation sequence of events with increasing and decreasing load and permits the evaluation of hardness (contact pressure) and reduced indentation modulus as a function of penetration depth.

All nanoindentation experiments were performed using the electrostatic transducer of the Hysitron triboscope attached to a scanning force microscope Nanoscope IV of Veeco. The transducer consists of a three plate capacitor, the mid-plate of which carries the impression tool fixed to a thin stylus. Application of a dc voltage generates an electrostatic force driving the indenter into the sample surface. Simultaneously the capacity change as a measure of penetration depth is recorded resulting in a force–depth curve. Additionally the indenter can be used for scanning over the sample surface for imaging. In our experiments a diamond cube corner is used (whose included angle is 90°) which generates a considerably high strain. For this reason the role of fracturing in the deformation mechanism will be important.

The nanohardness tester produces reasonable results for a load scale beginning at about 10 μN with a size of the impressed area of several nm; the maximum load is 10 mN. This is suited to study systems of reduced dimensionality and its application to thin ion irradiated layers is therefore very straightforward. Moreover, features of mechanical deformation at very low load can be studied which is also interesting for pristine MgO crystals. The standard procedure of Oliver and Pharr [13] is applied for the evaluation of hardness H and indentation modulus E. H represents the mean contact pressure under load and is obtained by the applied load F divided by the projected area A_C of the indenter tip at the corresponding contact depth h_c. The indentation modulus is derived from the slope of the force–displacement curve upon unloading as the material recovers elastically.

Depth dependent mechanical properties are easily achieved through indentation tests where repeated loading and unloading are performed at the same place on the sample surface [7,14] resulting in multi-cycling indents. After loading, the force is decreased to a load minimum, then the sample is reloaded to a maximum force. After onset of plastic deformation (yielding) the loading curve is an overlap of both plastic and elastic deformation. In contrast to this the unloading curve is commonly regarded as purely elastic. If the unloading curve is not purely elastic, hysteresis loops appear when reloading takes place. The analysis of the loops gives additional insight into the materials properties that might change due to the applied contact pressure from the tip. Thus the multi-cycling delivers a set of data which involves the entire material response from the first indenter-sample contact to the maximum penetration. Besides being time-efficient, the data collection method also does not suffer from lateral inhomogeneities of the sample.

Repeated unloading–reloading (multi-cycling) was performed in constant load repetition mode. In this mode reloading is always performed to the same maximum load. It is aimed at the study of possible irreversible contributions to the unloading/reloading that become manifest by a hysteresis loop. Such contributions may result from crack formation, phase transition, dislocation motion on unloading, interstitial hopping etc. In polymers, visco-elastic behaviour is very often the source of hysteresis loop generation [15]. In particular, the constant load repetition mode can be used to track the repeatability of the mentioned inelastic processes. If a phase transition is not reversible, a loop will only appear during the first cycle. When it is partially reversible, the loop area will show a certain damping from cycle to cycle.

Typical loading rates are a few μN/s up to a few mN/s. A change in measured contact pressure due to loading rate effects could not be observed. Holding segments at the beginning and end of the indentation are used to determine the thermal drift. The average value of drift speed was used for data correction. In such cases, where the difference of drift speed was larger than 0.05 nm s^{-1}, the indentation result was not used for further consideration.

3. Atomistic modelling

Fig. 1 shows a schematic representation of the model employed in the MD simulations. The model consists of an indenter attached to a vertical spring with a spring constant k_y. This model mimics the role of the cantilever in the SFM used for the experiments. The simulation consists of two main stages, namely, thermalisation and relaxation of the system and the indentation of the substrate.

The indenter has the configuration of a 90° triangular-based pyramid, and is constructed by taking a cubic diamond crystal with (100) faces and cutting along the diagonal (111) plane. The tip of the indenter is the vertex formed by three intersecting (100) faces and the most stable configuration is when the atoms on the three (100) planes are dimer reconstructed. Experimentally the tip is not atomically sharp and so curvature is also added to the indenter by truncating a number of atoms at the apex [10]. This adds a curvature radius of about 20 Å to the tip apex and reduces the apex length. The C–C interaction between the diamond indenter atoms are described by Brenner's many-body potential [16]. The indenter employed is configured from 8432 atoms and is orientated so that

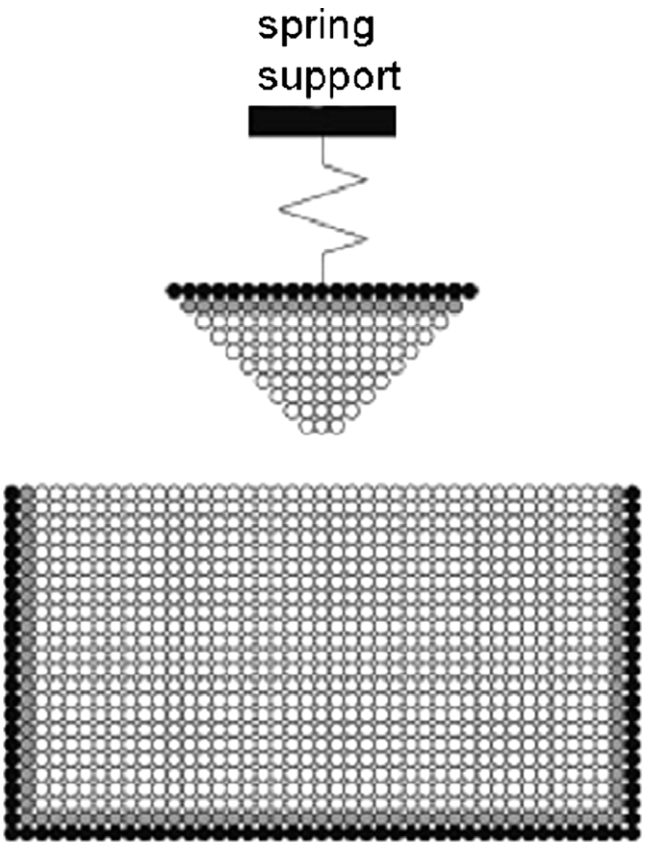

Fig. 1. Simulation model with the cross-section of the substrate and indenter with fixed (●), thermostat (◯) and free (○) atoms as indicated.

the tip moves with the (1 1 1) planes parallel to the surface of the substrate. The interaction between the tip and the substrate is modelled using the ZBL screened Coulomb potential [11]. The Mg–Mg, Mg–O and O–O potentials act pairwise and consists of the ZBL potential for short interactions splined to a Buckingham and Coulombic potential at greater distances. The parameters for this potential are given in reference [17]. A multipole method was employed to calculate the terms in the long ranged Coulomb sums.

The substrate takes the form of a cubic crystal lattice with the rock salt structure and a (1 0 0) surface. The lattice parameter for MgO is $a_0 = 0.421$ nm. For the initial indentation into the (1 0 0) surface of MgO, a cubic lattice of 144 000 atoms ($12.6 \times 8.4 \times 12.6$ nm) was used. Of these atoms, approximately 20 000 were fixed and 46 000 were thermalised. Size effects were assessed by running simulations first on smaller systems for shallower depths and then comparing the force–depth curves as the system size increased. The ultimate choice of size was a compromise between numerical convergence and available computational power. Both the indenter and the substrate consist of atoms that are fixed, thermalised or unconstrained (see Fig. 1). The thermalised atoms are attached to a Berendson thermostat to control the temperature and keep the temperature of the system at 300 K. The fixed atoms are the outer two layers of the substrate located on the vertical sides and those composing the two bottom layers. The top three layers of the indenter are also fixed and constrained to move by the vertical spring. The next three layers of the indenter and five layers of the substrate consist of thermalised atoms. The remaining atoms are unconstrained. The spring is connected to a support which is moved in a prescribed manner so that its displacement in the vertical direction is given by $y_B(t)$.

The indenter apex is first positioned outside the range of the tip–substrate interaction potential above the substrate surface (0.421 nm). The springs are connected to the atoms of the top few (1 1 1) planes of the indenter. These atoms are treated as a point mass that move together and experience an integrated vertical force F_y from all the atoms below in the indenter and also a force from the attached spring. During the indentation phase the fixed atoms are constrained in the horizontal and lateral directions. Thus, the equation of motion of this point mass during the indentation process is given by

$$ma_y(t) = F_y(t) + k_y(y_B(t) - y(t)), \quad (1)$$

where $a_y(t)$ is the vertical acceleration of the fixed indenter atoms at time t, m is the mass of the tip and $y(t)$ is the vertical displacement. The term $k_y(y_B(t)-y(t))$ is the spring force on the indenter.

The depth of the indentation was set to 1.2 nm and at this depth the indenter was held for 10 ps. The velocity of the indenter support during the indentation phase was held constant at 10 ms^{-1}, and during the retraction the same speed was used. In all our simulations, the classical equations of motion for all the atoms in the system were numerically integrated using the velocity-Verlet algorithm.

4. Results and discussion

4.1. Nanoindentation of non-irradiated MgO: experiment and molecular dynamic simulation

Nanoindentation into single crystalline non-irradiated MgO(1 0 0) results in three different typical areas shown from experiment in Fig. 2(a). The first characteristic feature was

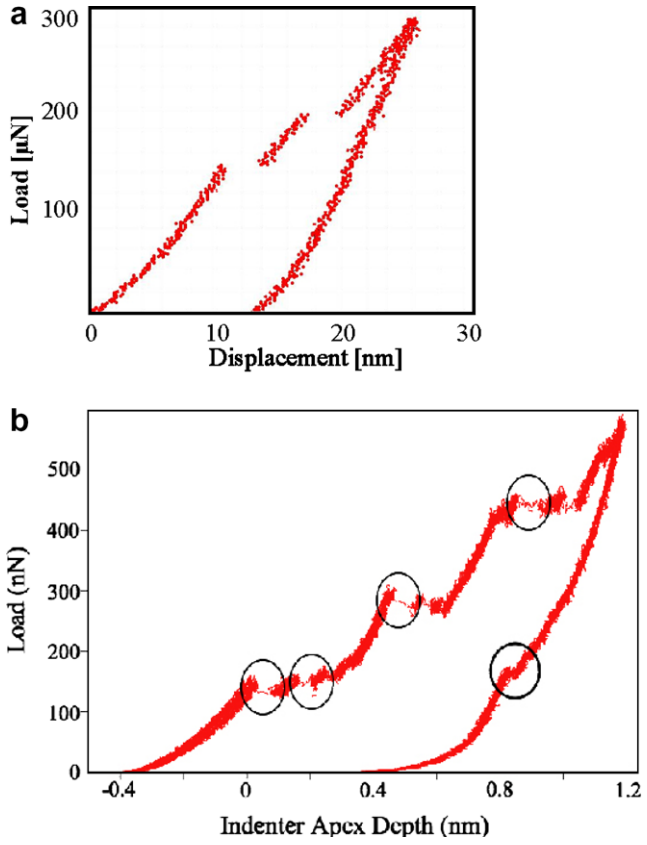

Fig. 2. Typical load–displacement curves for nanoindentation into MgO(1 0 0) (a) experiment with 300 μN maximum load and (b) simulation up to 1.2 nm indentation depth.

observed as elastic deformation without residual deformation at the very beginning of the indentation. Plastic deformation suddenly started with a typical pop-in at the critical load of 145 μN, referred to as the second typical process for mechanical deformation in MgO. The critical load for the first pop-in was confirmed by several reproducible indentation experiments on the same sample at different places on the surface. When the indentation was stopped just after the pop-in, the residual imprint depth corresponds exactly to the extent of the pop-in. For lower loads the deformation process is completely elastic, whereas the pop-in marks the beginning of plastic changes in the material. The contact pressure for the critical load for the first pop-in was calculated as 12.5 GPa. A similar scenario is given by Tromas et al. [4] for larger applied loads.

The penetration of the tip into the material continues with elasto-plastic deformation known as the third section during mechanical deformation. That third section can contain continuous elasto-plastic deformation, further pop-ins and finally cracks. The next pop-in in the example of Fig. 2(a) is visible at 200 μN. The pop-ins after the first one with the critical load, appear irregularly with smaller penetration depth during the pop-in. For loads larger than 5 mN cracks are visible with the indentation pattern observed with the scanning force microscope (SFM). The largest cracks were observed when indenting the (100) face and no cracks on the (111) face. The pop-ins could therefore be explained either in terms of the onset of slip in the slip planes inclined at 45° to the (100) surface or by the onset of subsurface micro-cracks along the slip planes that are perpendicular to the surface where cracking under larger loads has been observed. This is investigated in more detail in molecular dynamic simulations.

The molecular dynamic simulation results for indentation into MgO(100) are presented in the load–displacement curve of Fig. 2(b) and show a sequence of pop-ins with increasing load and a so-called 'pop-out' at the unloading curve. The contact pressure for the simulated force–depth curves shown in Fig. 2(b) was calculated and gives the value of 57 GPa, which is much larger than the experimental value of 12.5 GPa obtained from the present experiment. However, Tromas [3] estimated a theoretical value of 58 GPa and quote experimental values of 31 GPa and 27 GPa for a blunt and sharp indenter for a penetration depth of 70 nm. The larger values in the simulations compared to those from the experiment result at least in part from the fact that the boundaries of our simulation are fixed at fairly short distances and our tip is also much sharper. In addition the indentation depths are much smaller than experiment and often the contact pressure is larger at small indentation depths, known as the so called indentation size effect [14]. A recent paper has shown that the calculated contact pressure is reduced by a factor of 2 or more when the atomistic region is coupled to a finite element [18]. Another difference with experiment is the loading rate. This is a factor of about 10^9 times slower than the simulations and would have an important effect for materials where creep and time-dependent effects are important. However it is not expected to unduly affect the emission of dislocations in MgO which is a very fast phenomenon. However it could affect the growth of cracks. If cracks grow more slowly than the indentation speed then this could also explain the larger hardness calculated from the MD simulations compared to experiment. Rate effects are an important area of further study but are beyond the scope of this paper to address and the mechanisms by which cracks form should be further studied varying rate effects in larger scale MD simulations.

The 'pop-out' phenomenon is a sudden upwards movement of the indenter without any considerable change in contact force. This would suggest that there are a number of substrate atoms, which are undergoing recovery following the motion of the indenter. This type of recovery occurring during the pop-out phase is unlike the regular elastic recovery which can be recognised by a smooth, continuous unloading curve. The pop-out refers to a sudden reversible process during deformation of the material switching forward and backward the motion of atomic layers corresponding to load increase and decrease, respectively.

The initial part of the MgO force depth curve in the simulations (Fig. 2(b)) shows only elastic deformation. This portion of the curve conforms to a power law relationship of the form $F = Ch^m$, where F

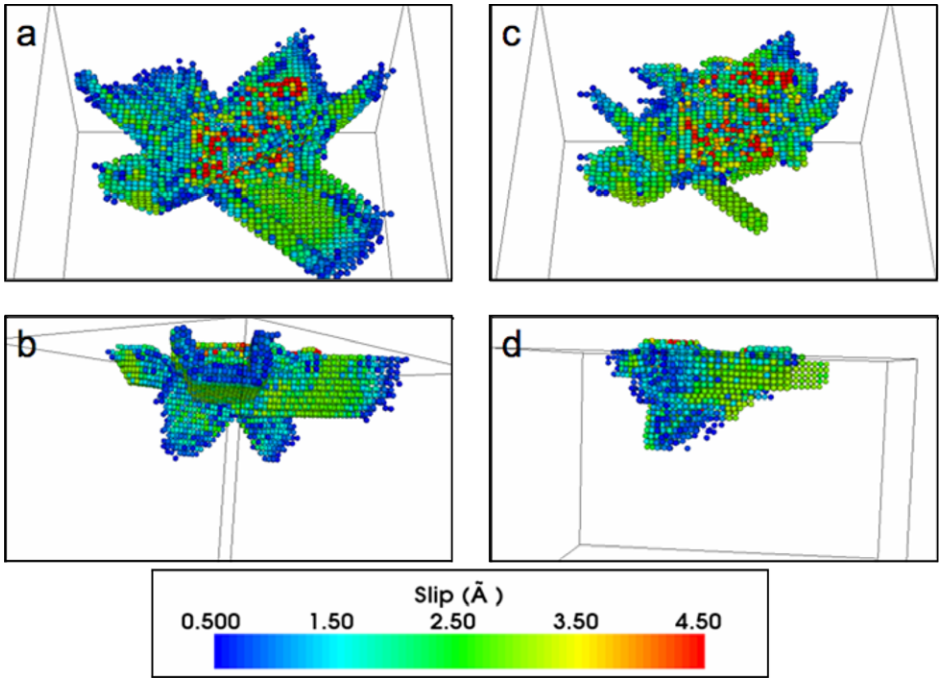

Fig. 3. Molecular dynamics simulation of the slip systems for nanoindentation in MgO(100). The images on the left are at peak indentation depth, and those on the right are after completion of the simulation.

and h are the load applied and the elastic displacement of the indenter, respectively where C and m are two constants. The simulations give a value of with $m = 1.93$ relevant for a conical indenter. During further indentation, defect generation beneath the tip is observed during simulation. Looking at the first pop-in, there is a significant change in the number of atoms that have moved in a slip plane at this event. All other slip events that occur show a similar jump in the number of atoms that move during these events. The pop-out seen in Fig. 2(b) corresponds to the sudden motion of atoms up onto the surface. This is highlighted by the arrow shown in Fig. 5.

Studying the movement of atoms during the indentation and retraction, definite slip planes can be seen to develop (Fig. 3). The slip is identified according to the scheme developed by de la Fuente et al. [20] which gives a measure of the amount an atom has moved relative to its neighbours. Multiple slip planes have been activated during the indentation with a significant number of atoms being subjected to movement along a number of planes. The atoms involved in slip do not move along the most densely packed directions, but charges of opposite type slide over each other and the slipped atoms move to a site previously occupied by an atom of the same species. Intermediate configurations are not so favourable as in metals because of the strong Coulombic interactions. The slip planes are therefore of the {1 1 0} type. There are six symmetrically equivalent {1 1 0} planes in MgO. When indenting the {1 0 0} surface, two of the six {1 1 0} planes can be described as being perpendicular to the surface. There are also four diagonal {1 1 0} type planes inclined at 45° to the surface. The atomistic simulations shown in Fig. 3 shows that the pop-ins have a length of around 0.2 nm, indicating a translation along the slip planes of one interatomic spacing. Slip occurs in directions of the <1 1 0> type within the slip planes.

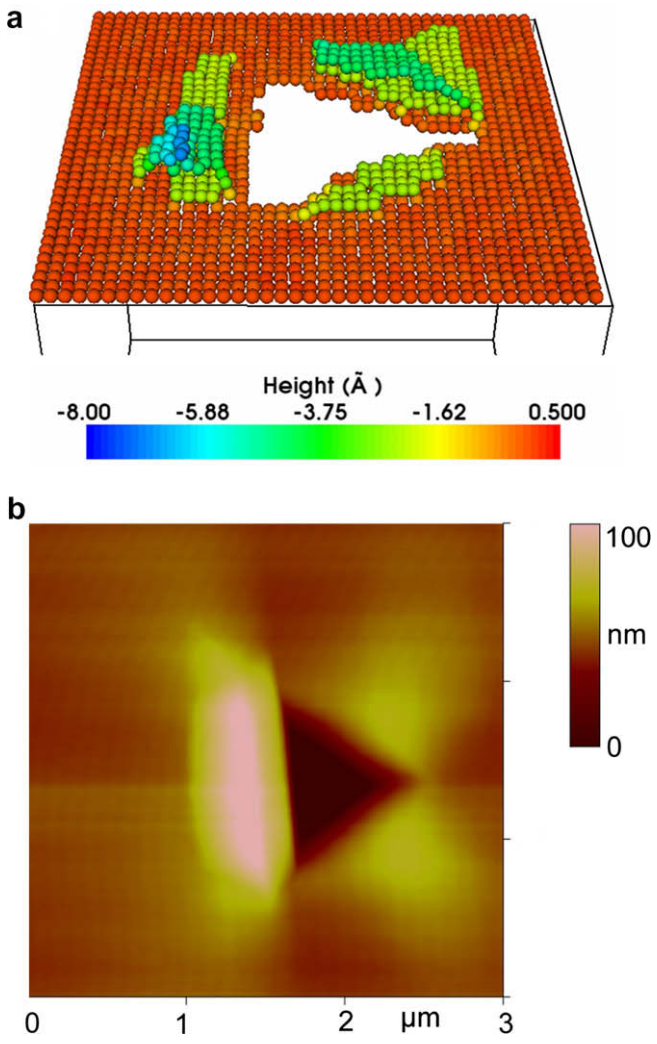

Fig. 4. Indentation imprint with pile-up pattern for MgO(1 0 0) (a) molecular dynamics simulation after an indentation depth of 1.8 nm: and (b) SFM image for 5 mN peak load.

Fig. 3 exhibits the slip systems that are activated during the indentation process. The images on the left are taken under peak load with the top image showing the four slip planes that intersect the surface normally with atoms moving away from the indent site in a horizontal direction. The image in the bottom left shows two significant {1 1 0} planes inclined at 45° to the surface which are activated beneath the other planes. The images on the right show the situation at the end of the simulation. At this point there has been a considerable retraction of the slip systems during the unloading stage. Upon completing the nanoindentation simulation, the surface of the substrate in the region of indentation shows a considerable pile up of material.

Fig. 4(a) shows that the matter accumulated on the surface around the indentation site piles up asymmetrically around the triangular imprint that is left. The pile on one side of the triangular indent does not extend outwards from the indentation site but is a strip 4–5 atoms wide running along the side of the indent. Here the pile up is generally higher and a maximum pile up of around 0.8 nm (4 layers) can be seen. The pile-up areas along the two other indent sides are only 2 layers in height. This can be compared with the experimental observations shown in Fig. 4(b).

After complete unloading the generated indents were mapped by scanning force microscopy using the indenter tip as scanning probe. The indents displayed distinct pile up around the impression groove on (1 0 0) surfaces. This pile up should on one hand represent the symmetry of the sample surface, on the other hand it is influenced by the symmetry of the tip. Thus one obtains an overlap of surface and indenter symmetry, resulting in a Moiré-pattern due to an overlap of 4-fold and 3-fold symmetry for the (1 0 0) surface (Fig. 4(b)). The triangle represents the indentation, particularly strong pile up is formed along one edge, whereas both of the other sides show pile-ups of much smaller height. After sample rotation by 30° counter clockwise, the strong piling up now appears along another side. We propose that the pile up occurs along the <0 1 0> or <1 0 0> directions where the (1 0 1) or (1 1 0) slip planes intersect the (0 0 1) surface.

The effects on the (1 0 0) surface of the slip systems in the simulations are compared looking at the pile up just after peak load and after complete retraction of the tip (Fig. 5).

The slip systems activated during the indentation causes the injection of circled half planes (Fig. 5) into the upper layers. Fig. 6 shows that these are classical edge dislocations with Burger's vector 1/2 (1 1 0) and a magnitude of 0.298 nm. As the indenter withdraws from the surface some of these half planes retract, however, a number of them remain. The half planes have caused the surface to be raised slightly causing a small mound which remains. Khan et al. [1] saw a similar pattern as a result of cracking during high force Vickers indentation experiments. It is likely that any cracks, that do form in MgO under high pressure testing, are formed due to the behaviour of the slip planes perpendicular to the surface causing the injection of these half planes in the material.

In order to check experimentally irreversible features during nanoindentation, multi-cycling indentation was applied. Generally loops will appear in the load–displacement curve if permanent changes in the structure happen that are different from a completely elastic recovery of the material after retraction of the tip. Load–displacement curves for multi-cycling indentation in the

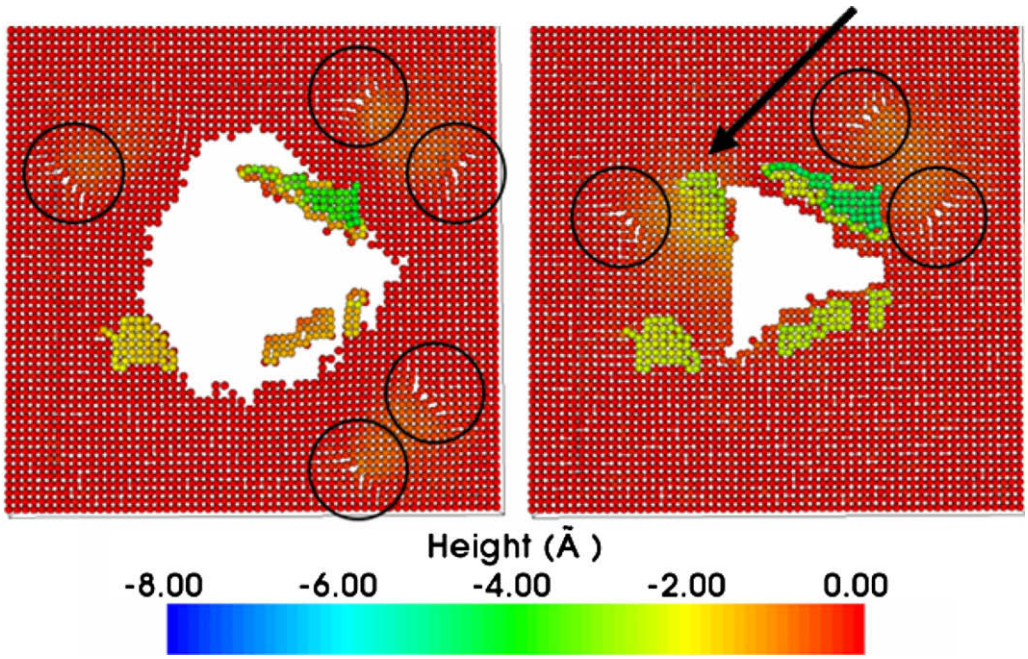

Fig. 5. Simulation results for indentation into MgO(100) to an indentation depth of 1.2 nm: the image on the left is just after peak indentation depth and the right image is after completion of the simulation. Circled areas show the extra half planes caused by the slip systems. The arrow marks additional piling up after retraction of the tip which is also visible as pop-out in the load–depth curve of Fig. 2(b).

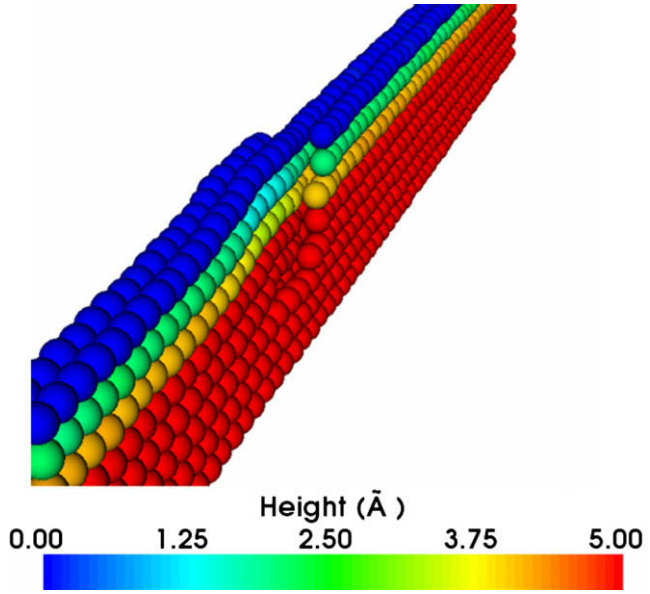

Fig. 6. Simulation result with the termination of a horizontal half plane in the foreground, with the planes behind shaping around it. The top five layers of atoms have been subjected to slip and caused this half plane, the layers below showing minimal movement from their original positions.

constant load repetition mode for MgO(100) crystals are given in Fig. 7(a). Beside a dominant pop-in feature, loops are observed. The loop area is equivalent to an energy and exhibits a large decrease from cycle 1 to cycle 2, with a smaller tendency of further decline for the next few cycles, finally reaching a saturation value (see Table 1). A possible explanation is that during cycle 1 cracks are formed which propagate a little further within the next cycles. After about 5 cycles the loop area represents the energy necessary for opening and closing the non-propagating crack on loading/unloading. This scenario is reflected in the MD simulation with the generation of half planes that retract partly after removal of the tip (see Fig 5).

Surface cracks visible by microscopy investigations are not observed for applied loads up to 10 mN as used in our nanoindentation experiments. However other authors report on visible surface and also sub-surface cracks for larger applied loads that are easily visible in MgO during light microscopy investigations due to the transparency of the material [1,2]. A feature of nanocracks is the appearance of a hysteresis loop in multi-cycling nanoindentation. That is demonstrated in Fig. 7.

4.2. Nanoindentation of ion irradiated MgO

After Ar^+ ion irradiation 5 distinct differences to the untreated state were found:

- The hardness was increased for all surfaces.
- No pop-in event could be detected after ion bombardment.
- Hysteresis loops either do not appear or have drastically reduced area as long as the penetration depth did not exceed the thickness of the ion modified layer.
- The pile-up around the impressions was reduced and appeared in a more homogeneously distributed form.

Table 2 leads to the conclusion that the hardness anisotropy initially existing in the perfect crystal is reduced with increasing ion fluence and disappears completely for a fluence of 1×10^{20} Ar^+/m^2 and higher. We attribute this observation to the fact that the generated defects block the dislocation motion, but otherwise contribute to the mechanical deformation by mechanisms known to act in glass, amorphous matter and other less ordered material (point defect assisted inelastic deformation). It is obvious that these deformation mechanisms are rarely orientation dependent, hence resulting in an increasing loss of hardness anisotropy with growing disorder. These findings are also confirmed by the fact that after irradiation the pile up around the indent is decreased in volume and more homogeneously distributed.

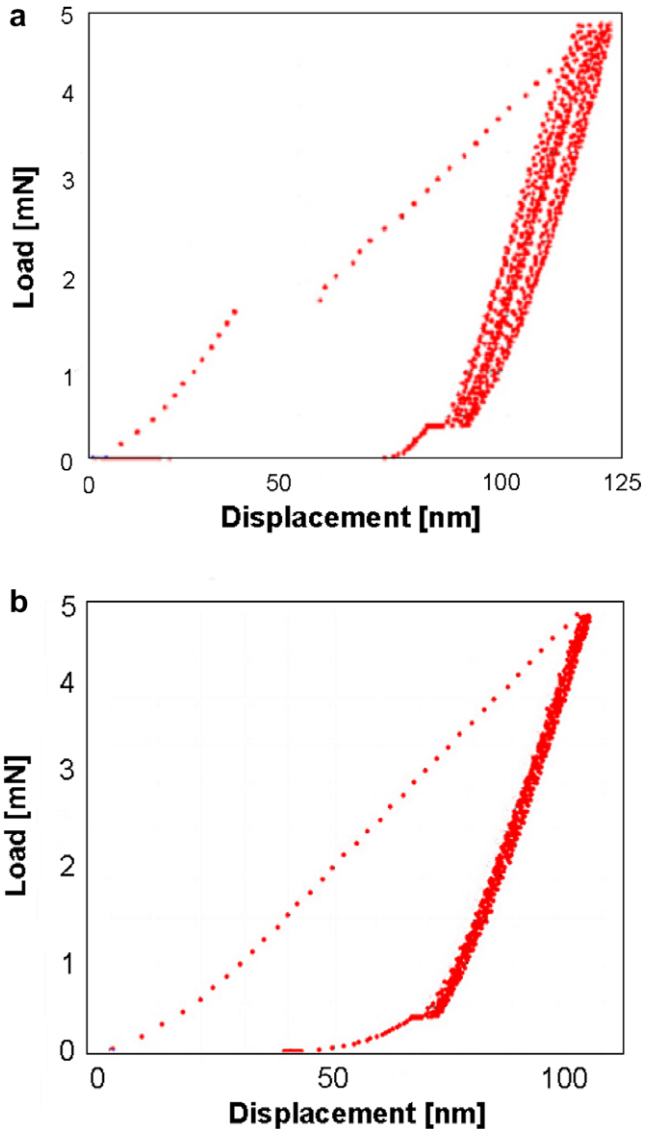

Fig. 7. Experimental load–displacement curves for multi-cycling nanoindentation in the constant load repetition mode (10 cycles) for 5 mN maximum load in MgO(100) for (a) pristine non-irradiated crystals and (b) irradiated samples with a fluence of 1×10^{20} Ar^+/m^2.

Table 1
Irreversibly consumed mechanical energy during unloading–reloading cycles (constant maximum force F_{max} = 5 mN) on the MgO(100) surface

Cycle number	1	2	3	4	6	8	10
Loop energy (10^{-12} J)	25	10	8	7	6	6	6

The table shows that the surface orientation effects have disappeared at the lower fluence but that there is still a hardness increase as the fluence is increased to 1×10^{20} Ar^+/m^2.

It was also found, that the formation of hysteresis loops is suppressed within the ion distorted layer (Fig. 7(b)). In our opinion, point defect assisted mechanisms will reduce the critical stress for inelastic deformation in the sample, thus reducing the formation of nano-cracks. Radiation damage increases the hardness but also the crack resistance. This is important from the viewpoint of practical application since there is some interest in the combination of such properties as high hardness and good fracture toughness. In comparison to the unirradiated samples the pop-ins disappear and a smooth load–depth curve is obtained.

Table 2
Evolution of hardness for non-irradiated and Ar^+ irradiated MgO for several surface orientations

Orientation status	(100)	(110)	(111)
Non-implanted	12.5 ± 0.7	13.5 ± 0.8	14.5 ± 0.7
0.5×10^{19} Ar^+/m^2	17.0 ± 0.9	16.7 ± 1.0	17.2 ± 0.9
1.0×10^{20} Ar^+/m^2	18.7 ± 1.0	18.9 ± 0.9	18.8 ± 0.9

The presented data were obtained by averaging several multi-cycling measurements in the depth interval between 60 nm and 100 nm.

4.3. Defects in MgO after irradiation

Recent simulation studies [19] have shown that both the cation and anion interstitials and the di and tri-interstitials are highly mobile within the lattice at room temperature and diffuse either combining with existing vacancies or forming interstitial clusters. The vacancies themselves on the other hand are highly stable and do not move. Some small interstitial clusters, e.g. the tetramer were also found to be stable but if such a cluster was to combine with a mobile di-interstitial, the cluster again became mobile with a preferred diffusion in the <110> direction, the same direction in which slip occurs. Interstitial clusters might therefore assist slip along the <110> direction by their ability to glide through the lattice in the same direction as which slip occurs. Thus it is suggested that it is the presence of the stable vacancies and vacancy clusters that will pin the dislocations causing the hardness increase. This hypothesis will be tested in the future by carrying out MD simulations into an MgO crystal with a large defect density.

5. Conclusion

An investigation of the mechanical properties of MgO(100) single crystals before and after irradiation has been carried out. For the nanoindentation process of non-irradiated MgO(100) crystals, molecular dynamic simulations have been performed, which support strongly the model of {110} type slip planes. The pop-ins can be explained in terms of the onset of slip in the slip planes inclined at 45° to the (100) surface leading finally to typical pile-up pattern that reflect the superposition of the stress fields of the crystal and the indenter. In the pristine samples repeated loading–unloading-cycles revealed the appearance of hysteresis loops that are related to nanofracturing. This can be correlated with the injection of extra half planes during the tip penetration. These half planes retract as the indenter is withdrawn from the surface, but a few remain.

For the Ar^+ irradiated samples, the hardness was increased for all surface orientations of the MgO crystal and no pop-in event could be detected after ion bombardment. The observed hardness changes with depth are due to the inhomogeneous distribution of point defects generated during irradiation. No hysteresis loop in the force–displacement curve was formed with multi-cycling after implantation. This is explained in terms of point defect assisted plasticity.

Acknowledgements

This work was carried out in conjunction with a Royal Society joint project grant between the UK and Germany (e-GAP 2005/RI-JP) for which funding is gratefully acknowledged. We would also like to acknowledge support from the EPSRC (EP/C524322/1), which has provided funding for one of us (I.G.).

References

[1] M.Y. Khan, L.M. Brown, M.M. Chaudhri, J. Phys. D: Appl. Phys. 25 (1992) A257.
[2] Y.S. Boyarskaya, R.P. Zhitaru, D.Z. Grabko, V.A. Rahvalov, J. Mater. Sci. 33 (1998) 281.

[3] C. Tromas, J. Colin, C. Coupeau, J.C. Girard, J. Woirgard, J. Grilhe, Eur. Phys. J. AP 8 (1999) 123.
[4] C. Tromas, J.C. Girard, V. Audurier, J. Woirgard, J. Mater. Sci. 34 (1999) 5337.
[5] P.F.M. Terán Arce, G. Andreu Riera, P. Gorostiza, F. Sanz F, Appl. Phys. Lett. 77 (2000) 839.
[6] D. Caceres, I. Vergara, R. Gonzalez, Y. Chen, Nucl. Instrum. and Meth. B 191 (2002) 178.
[7] A. Richter, B. Wolf, M. Nowicki, R. Smith, I.O. Usov, J.A. Valdez, K. Sickafus, J. Phys. D: Appl. Phys. 39 (2006) 3342.
[8] J. Li, A.H.W. Ngan, P. Gumbsch, Acta Mater. 51 (2003) 5711.
[9] D. Christopher, R. Smith, A. Richter, Nanotechnology 12 (2001) 372.
[10] R. Smith, D. Christopher, S.D. Kenny, A. Richter, B. Wolf, Phys. Rev. B 67 (2003) 245.
[11] J.F. Ziegler, J.P. Biersack, U. Littmark, The Stopping and Range of Ions in Solids, Pergamon, New York, 1985.
[12] A.C. Fischer-Cripps, Nanoindentation, Springer-Verlag, New York, 2002.
[13] W.C. Olivier, G.M. Pharr, J. Mater. Res. 7 (1992) 1564.
[14] B. Wolf, A. Richter, New J. Phys. 5 (2003) 15.1.
[15] M. Nowicki, A. Richter, B. Wolf, H. Kaczmarek, Polymer 44 (2003) 6599.
[16] D.W. Brenner, Phys. Rev. B 42 (1990) 9458;
D.W. Brenner, Phys. Rev. B 46 (1992) 1948.
[17] B.P. Uberuaga, R. Smith, A.R. Cleave, F. Montalenti, G. Henkelman, R.W. Grimes, A.F. Voter, K.E. Sickafus, Phys. Rev. B 71 (2005) 102.
[18] E. Mcgee, S.D. Kenny, R. Smith, Int. J. Mater. Res. 98 (2007) 430.
[19] I.O. Usov, P.N. Arendt, J.R. Groves, L. Stan, R.F. DePaula, Nucl. Instrum. and Meth. B 240 (2005) 661.
[20] O.R. de la Fuente, J.A. Zimmerman, M.A. Gonzales, J. de la Figuera, J.C. Hamilton, W.W. Pai, J.M. Rojo, Phys. Rev. B 88 (2002) 036101.